

Giant shifts of crystal-field excitations in ErFeO₃ driven by internal magnetic fields

Joel O'Brien,¹ Guochu Deng,^{2*} Xiaoxuan Ma,³ Zhenjie Feng,³ Wei Ren,³ Shixun Cao,^{3†} Dehong Yu,² Garry J McIntyre,² Clemens Ulrich¹

¹ School of Physics, The University of New South Wales, Kensington, NSW 2052, Australia

² Australian Centre for Neutron Scattering, Australian Nuclear Science and Technology Organisation,
New Illawarra Road, Lucas Heights, NSW 2234, Australia

³ Department of Physics, International Centre of Quantum and Molecular Structures and Materials Genome Institute,
Shanghai University, Shangda Road 99, Shanghai 200444, People's Republic of China

Crystal-field excitations in transition-metal oxides where -rare-earth elements locate in the space between the transition-metal-oxide tetrahedra and octahedra, are assumed to be robust with respect to external perturbations such as temperature. Using inelastic neutron-scattering experiments, a giant shift of the energy of the lowest crystal-field excitation of Er³⁺ (⁴I_{15/2}) in ErFeO₃ from 0.35 meV to 0.75 meV was observed on cooling from 10K to 1.5K through the magnetic ordering temperature of Er³⁺ at 4.1 K. A crystal-field model was proposed to explain the observed crystal field excitations in this work. The model indicates the lowest-energy crystal-field excitation in ErFeO₃ is the first Kramers doublet above the ground state. Its energy substantially shifts by the internal field induced by the ordered Er³⁺ magnetic moments. Further magnetic-field-dependent measurements provide strong supportive evidence for this scenario. By fitting the external magnetic-field dependency of the crystal-field excitation energy, the internal field generated by Er³⁺ magnetic moments was derived to be ~0.33meV. The result indicates that the internal field of Er³⁺ magnetic moments contribute to the energy shift of the crystal-field excitations. The giant energy shift under fields could be attributed to the anisotropy of the large effective *g*-factor.

PACS number(s): 71.70.Ch, 78.70.Nx, 75.85.+t, 75.25.+z

* Corresponding Author: guochu.deng@ansto.gov.au

† Corresponding Author: sxcao@shu.edu.cn

I. INTRODUCTION

In transition-metal oxides (TMO), the interplay and competition of spin, charge, and orbital degrees of freedom result in a plethora of fascinating effects such as high-temperature superconductivity, colossal magnetoresistance, frustrated magnetism, multiferroicity, etc. The complexity of magnetic exchange interactions leads to a large variety of exotic magnetic ground states in these compounds, such as commensurate/incommensurate magnetic structures,¹ and frustrated quantum spin liquids². A rare-earth TMO perovskite consists of a network of corner-sharing MO_6 octahedra with a rare-earth element filling the cuboctahedra in-between. Magnetic properties of rare-earth TMO perovskites are mainly dominated by the exchange interactions between the transition-metal sublattice in the intermediate/high temperature range. While rare-earth ions start to play important roles in the low-temperature range, where rare-earth spins start to interact with the transition-metal spins and induce extra magnetic polarization in the magnetic order on the transition-metal sublattice, and even cause magnetic phase transitions in some cases. Certain rare-earth ions tend to form long-range magnetic orders at very low temperature as well.^{3,4}

In rare-earth compounds, the symmetric Coulomb potential generated by the surrounding cations causes lifting of the degeneracy of the rare-earth $4f$ electron levels. The crystal-field (CF) effect of rare-earth ions can be considered as a perturbation to the lowest-energy multiplets of $4f$ ions.⁵ The corresponding CF excitations in these compounds fall into an energy range from a few meVs to hundreds of meVs, comparable with the cold- or thermal-neutron energy, and thus can be observed by inelastic neutron scattering⁶⁻⁸, as an alternative method to solid-state spectroscopy such as electron spin resonance⁹ or infrared spectroscopy¹⁰⁻¹². CF excitations are generally considered as local phenomena (nondispersive) due to the weak and almost negligible interaction between the neighbouring rare-earth ions. Due to the Zeeman effect, CF excitation energies could vary by applying external magnetic fields or inducing internal fields by forming long-range magnetic ordering. Boothroyd *et al.* suggested that the shifts in CF energies could even be used as a sensitive probe, i.e. ‘crystal field spectroscopy’ to determine the local electrical or magnetic fields on the rare-earth ion sites.¹³

Numerous experiments were performed in the past decades to study CF excitations in compounds with various local symmetries. Using inelastic neutron scattering, Loewenhaupt *et al.*^{6,8} discovered energy shifts and linewidth narrowing in the CF excitations of Ce^{3+} with temperature in the LaAl_2 matrix and other lanthanide-alloy compounds. The temperature-driven linewidth change was observed in metallic rare-earth systems and explained as the damping effect of conduction electron-hole excitations by Becker *et al.*¹⁴ Abrupt decreases of the CF excitation linewidths in $\text{La}_{1-x}\text{Tb}_x\text{Al}_2$ ⁷ and $\text{PrOs}_4\text{Sb}_{12}$ ¹⁵ were observed below their superconducting phase transitions using inelastic neutron scattering and were attributed to a suppressed electron scattering due to the opening of the superconducting gap. A similar linewidth shrinkage in $\text{Pr}_2\text{O}_2\text{M}_2\text{OSe}_2$ ($\text{M} = \text{Mn}, \text{Fe}$) below their magnetic ordering temperature was attributed to the opening of the spin-wave gap at the zone centre by Oogarah *et al.*¹⁶ CF-level splitting was widely studied in Nd_2CuO_4 ¹⁰, NdMnO_3 ¹¹, $\text{RFeAsO}_{1-x}\text{F}_x$ ($\text{R} = \text{Pr}, \text{Nd}$)¹⁷, YbMnO_3 ¹⁸, HoMn_2O_5 ¹⁹, and DyMnO_3 ¹². The underlying mechanism of CF splitting strongly depends on the magnetic interactions. It is highly interesting to study CF splitting in rare-earth CMOs since it can provide profound insights into the complicated magnetic interactions of these magnets.

Rare-earth orthoferrites $RFeO_3$ (R denotes a rare-earth element) demonstrate intriguing magnetism on the two magnetic sublattices of Fe^{3+} and R^{3+} .^{4,20} Novel properties,²¹⁻²⁴ such as ultrafast laser responses,²⁵ and multiferroicity,^{21,24} were recently discovered in rare-earth orthoferrites, reviving research interests in this series. The members have similar orthorhombically distorted perovskite crystal structures⁴, described by space group $Pbnm$.³ The Fe^{3+} sublattice forms a canted long-range antiferromagnetic (AFM) magnetic structure at $T_{N(Fe)}$ between 600K and 740K.⁴ In most $RFeO_3$, a spin-reorientation transition (SRT) takes place at a lower temperature T_{SR} or in a temperature regime between T_l and T_u . The R^{3+} magnetic moments in some $RFeO_3$ order at a much lower temperature $T_{N(R)}$, near the liquid-helium temperature.³ It is generally believed that the magnetic behaviour of $RFeO_3$ is a combined result of the interactions of Fe^{3+} - Fe^{3+} , R^{3+} - Fe^{3+} , and R^{3+} - R^{3+} . Single-ion anisotropy and weak antisymmetric exchange interaction play additional roles.^{4,26}

CF excitations were widely observed and studied in $RFeO_3$. The spin-orbital coupling splits the outermost $4f$ electrons into multiplets. Er^{3+} has an electron configuration of $4f^{11}$ with the lowest multiplet $^4I_{15/2}$, which splits into different doublets and quartets due to the local symmetry.²⁷ Even though the CF excitation was previously observed in $ErFeO_3$, no careful analysis has been done so far. Recently, Zic et al. reported a slightly dispersive CF excitation due to the exchange between the Er^{3+} and Fe^{3+} sublattice at low temperature.²⁸ Here we attempt to study the CF excitations in $ErFeO_3$ using the inelastic neutron-scattering technique and demonstrate or derive the effects of external and internal magnetic fields on the CF excitation in this compound.

In this study, the low-energy magnetic excitation modes were measured in $ErFeO_3$ over a wide temperature range from 1.5K to 150K. The CF excitations from Er^{3+} in $ErFeO_3$ were observed and the results were fitted to a CF Hamiltonian by using Stevens operator equivalents. Energy shifts of the CF excitations were observed upon the ordering of the Er^{3+} magnetic moments. The magnetic-field dependency of the lowest CF excitation was systematically measured, and a strong shift of the excitation energy was observed under external magnetic fields. Such strong internal and external magnetic-field effects are modelled and explained in detail.

II. EXPERIMENTAL DETAILS

The $ErFeO_3$ single-crystal sample in this study was grown by using the optical floating-zone furnace (FZ-T-10000-H-VI-P-SH, Crystal Systems Corp.) in the Department of Physics at Shanghai University. We performed the inelastic neutron-scattering experiments on the cold-neutron triple-axis spectrometer Sika²⁹, the thermal-neutron triple-axis spectrometer Taipan³⁰, and the time-of-flight (TOF) spectrometer Pelican³¹ at the Australian Centre for Neutron Scattering (ACNS), Australian Nuclear Science and Technology Organisation (ANSTO). On Sika, a constant- E_f mode with $E_f = 5\text{meV}$ and 60° - 60° - 60° - 60° collimation was configured for the experiment. A cooled Be-filter was used to remove the second-order contamination in the scattered neutron beam. On Taipan, we used full open collimation and the constant- E_f mode ($E_f = 14.87\text{meV}$) as the configuration. A 4cm-thick PG (200) filter was placed in front of the pre-analyser collimator to suppress the high-order wavelength contamination. The sample was cooled to the desired temperature using

a He-flow cryostat, which was controlled by a Lakeshore 340 temperature controller. The data from both Sika and Taipan were fitted by convoluting with the instrumental resolutions of the configurations mentioned above. The software Octave³² and the software package Reslib3.4³³ were used for the data fitting. The Pelican experiment was carried out with an incident neutron of wavelength = 3.65Å. A closed-cycle refrigerator was used to maintain the sample temperature. The Pelican data were treated by using the neutron-data-visualization software LAMP. The CF excitation was fitted by a least-square-minimization python code based on the crystal-field calculation package PyCrstyalField³⁴.

III. RESULTS AND DISCUSSION

A. Temperature dependency of low-energy crystal-field excitation

Inelastic neutron scattering experiments were carried out on the cold-neutron triple-axis spectrometer Sika and the results are displayed in Fig. S1 and S2 in the Supplemental Materials. Fig. S2(a), (b) and (c) reveal two main features in the excitation spectrum of ErFeO₃ in the energy range below 10meV. The first feature is the low-energy part of the spin-wave excitation at the zone centre from the Fe³⁺ sublattice, while the other one is the nondispersive excitation at ~5.4meV, which was confirmed to be a CF excitation from Er³⁺. Additionally, another low-energy excitation below 1meV was also observed in ErFeO₃ on Sika (Fig. S1), which shows no dispersion, and thus is attributed to another CF excitation from Er³⁺. This peak shows a strong temperature dependency at low temperature, especially, on cooling from just above the magnetic ordering temperature of Er³⁺ ($T_{N(Er)}$).

In order to determine precisely the temperature dependency of this lowest-energy excitation peak, we measured the scattering with energy transfer from -1 meV to 1 meV on Pelican from 1.7 K to 10 K with 0.1 K per step. A contour map of the intensities was constructed by combining all these scans and is shown in Fig. 1, and the corresponding raw data are shown in Fig. 2(a). The result at each temperature is the summation over the full experimentally accessible Q range in the Brillouin zone. The strong peak at zero energy transfer corresponds to the elastic scattering from the sample. The linewidth of this peak was taken to be the instrumental resolution for this configuration. A strong excitation peak was observed around 0.75 meV at 1.5 K. This peak shows no dispersion, which is verified by inspecting energy slices at the different Q cuts selected from the three-dimensional $S(Q, \omega)$ data generated from the Pelican experiment. This result is consistent with the experimental results collected on Sika, as presented in the Supplemental Materials.

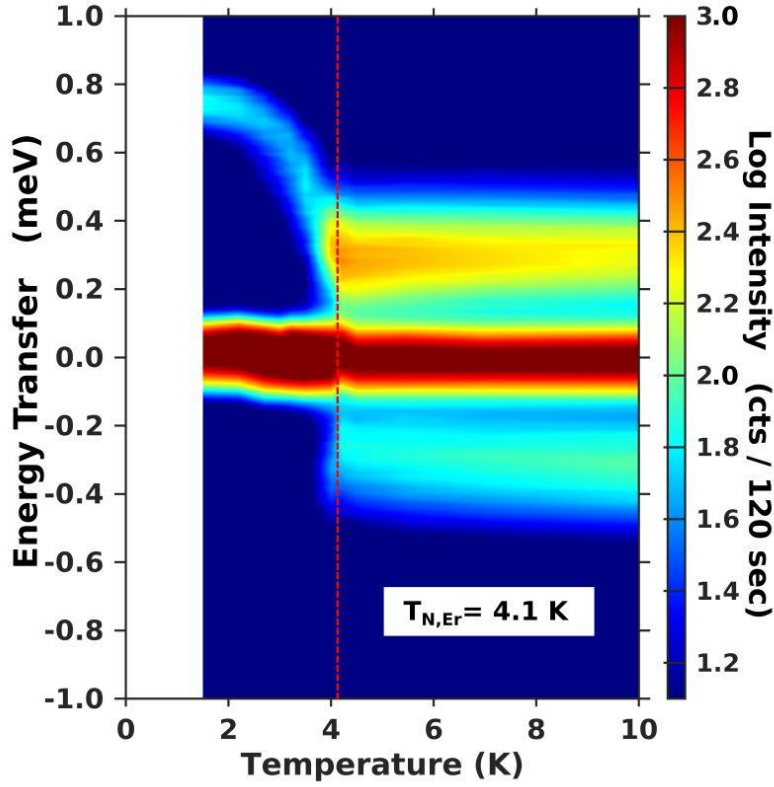


FIG 1 (color online) False-colour contour map of the intensities of the inelastic neutron scattering data of ErFeO_3 measured on the time-of-flight spectrometer Pelican at ANSTO at selected temperatures above and below the magnetic ordering temperature $T_{N(\text{Er})} = 4.2$ K of the Er^{3+} spins, as marked by the red vertical dashed line. The excitation visible at ± 0.35 meV at 10 K is attributed to a CF excitation. Its energy increases substantially below $T_{N(\text{Er})}$ while its integrated intensity and linewidth decrease. The central peak at zero energy transfer is due to elastic scattering from the sample. Note, the intensity is plotted on a logarithmic scale.

When heating the sample gradually from the base temperature (~ 1.5 K) to the antiferromagnetic ordering temperature ($T_{N(\text{Er})}$) of Er^{3+} , the excitation energy decreases step by step to ~ 0.35 meV at $T_{N(\text{Er})} = 4.2$ K. On further heating, the excitation energy of this peak does not show strong temperature dependency up to 10K. The temperature dependency of the excitation energy is displayed in Fig. 2(b). In contrast to the single excitation peak below $T_{N(\text{Er})}$, the CF excitation was observed on both the energy-loss and the energy-gain sides at these temperatures, which correspond to the Stokes and anti-Stokes excitations, respectively. This can be explained by the fact that there are more spins occupied in the excited states of this CF energy level when the temperature becomes higher than $T_{N(\text{Er})}$, which allows them to transfer energy to the neutrons and jump back to the low-energy state. The excitation energy demonstrates a similar temperature dependency as the magnetic moment of Er^{3+} obtained by neutron powder diffraction.³ Such a similarity from the base temperature to 10K undoubtedly indicates that this CF excitation has a strong correlation with the ordering state of Er^{3+} spins. The energy shift driven by the ordering of Er^{3+} is quite large, which is highly interesting and has never

been reported in similar magnetic compounds. It is immensely worthwhile to dig out the underlying mechanism of this phenomenon.

In addition to the energy shift, the linewidth and intensity of the excitation decreases significantly below the magnetic phase transition $T_{N(Er)}$, as shown in Fig.2 (c) and (d), respectively. Narrowing of the linewidth of this excitation could be attributed to the suppressed thermal fluctuation of the Er^{3+} magnetic moments below $T_{N(Er)}$, as pointed out in the literature by Berker et al.¹⁴ The abrupt decrease of the intensity at the transition is obviously due to the ordering of Er^{3+} spins. Below $T_{N(Er)}$, the peak intensity of this CF excitation increases upon further cooling. Similar temperature dependency was widely observed in other rare-earth systems^{35,36}

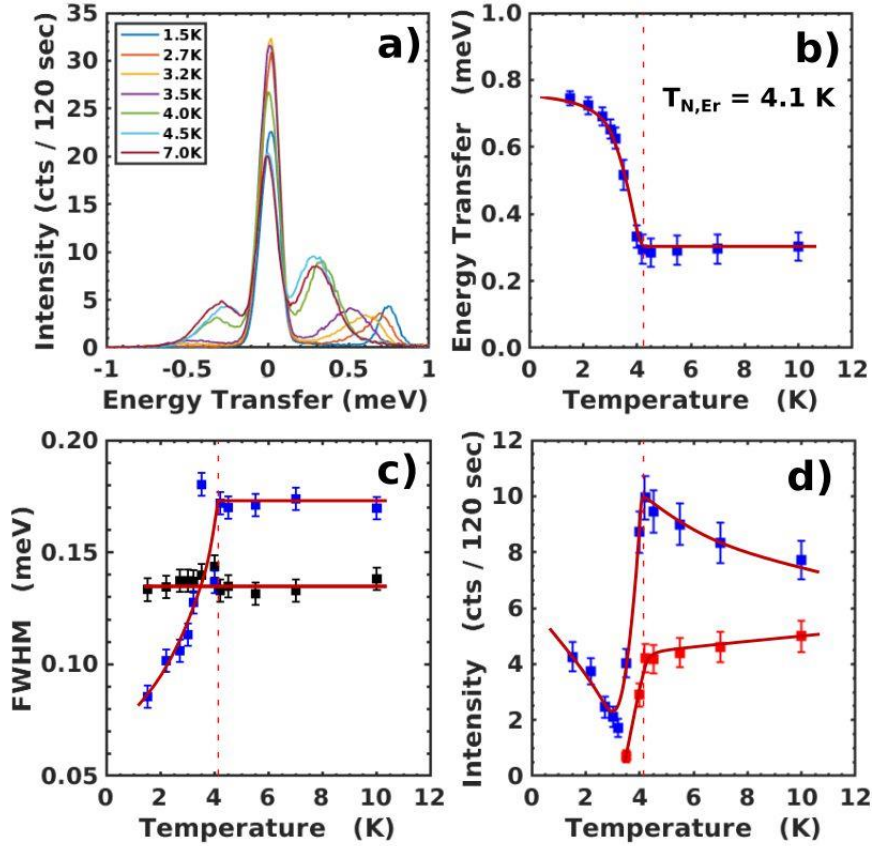


FIG 2 (color online) Temperature dependence of the low-energy CF excitation of $ErFeO_3$. (a) excitation spectrum at selected temperatures, (b) energy of the CF excitation versus temperature as determined by fitting a Pseudo-Voigt function to the experimental data. The vertical red line corresponds to the temperature of the magnetic phase transition of the Er^{3+} ions, $T_{N(Er)} = 4.1$ K, (c) linewidth (FWHM) of the CF excitations (blue symbols) and the linewidth of the central elastic line (black symbols) obtained from a Gaussian fit, as a function of temperature, (d) intensity of the Stokes (blue symbols) and anti-Stokes (red symbols) CF excitation peaks as a function of temperature. The red lines serve as guides to the eye.

B. Crystal Field Model of Er³⁺ in ErFeO₃

In order to understand the mechanism of the large energy shift of the CF level described above, further measurements and modelling are necessary. As mentioned in the previous section, the excitations from ErFeO₃ were measured in the energy-transfer range from 0 to 10 meV at temperatures from 1.5 K to 150 K, shown in Fig. S2. These results show the energy shift of another CF excitation level at ~5.5 meV. Further measurements at more temperature steps from 10K to 150 K in the same energy range show another nondispersive excitation peak at 7.5 meV, which increases in intensity with increasing temperature. In contrast, the intensity of the peak at 5.5 meV decreases at the same time upon increasing temperature. Thus, we speculate that the peak at 7.5 meV corresponds to a CF excitation from one excited state to another of ErFeO₃. (see the detailed discussion upon Fig. S4 and Fig. S5 in the Supplemental Material) A sound CF model is definitely needed to validate this speculation. Following this idea, a scan with a wider energy-transfer range was conducted at 1.5 K on the thermal-neutron triple-axis spectrometer Taipan in order to observe more CF excitations. Fig. 3 shows the wide-energy data from 1meV to 30meV at an off-centre Q position, which reveals four intense peaks at ~5.5 meV, ~13.3 meV, ~18 meV and ~25 meV (see Fig. S6). These observed CF excitation levels are consistent with the previously published fluorescence results.³⁷ Considering these CF excitations, we attempt to build a CF model for Er³⁺ in ErFeO₃.

The CF excitation of 4*f* ions can be mainly considered as a perturbation of its lowest-energy multiplet because the spin-orbital coupling is much stronger than the CF effect in 4*f* ions. Er³⁺ has a ⁴I_{15/2} ground state and the first excited state is ⁴I_{13/2}. Since Er³⁺ is a Kramers ion, the Er³⁺ ground state multiplet split into two doublets (Γ₆ and Γ₇) and three quartets (Γ₈) in a cubic CF symmetry.³⁸

Ammerlaan and de Maat-Gersdorf studied the Er³⁺ CF splitting in different local symmetric situations, such as cubic, trigonal, tetragonal and orthorhombic fields.³⁹ According to their numerical results, the orthorhombic CF can be described as a perturbation of the tetragonal symmetry, which is denoted by an extra term in the Hamiltonian. All multiplets in orthorhombic symmetry are split into eight Kramers doublets except for some accidental degeneracies. Following the same logic, a small distortion of lower symmetry can be considered as a perturbation of the orthorhombic CF. This method was successfully used to describe the CF excitation of Er³⁺ on the interstitial sites.³⁸ In ErFeO₃, Er³⁺ occupies the 4e Wyckoff position and has a Cs point group. Despite such a low symmetry, the CF still splits into eight Kramers doublets, just as in an orthorhombic environment.³⁹ In order to fit the CF parameters and avoid overparameterization, we limit the number of parameters for ErFeO₃ and adopt the Stevens operator equivalents of the orthorhombic symmetry as an approximation. In the research on single-molecule magnets, the theoretical models normally only consider the symmetry of the point charge around the central magnetic ions, but disregard the actual molecular geometries of surrounding ligands.⁴⁰ A similar simplification in the current study is adopted as the first step in order to achieve stable initial-fitting parameters to the data.

The CF Hamiltonian commonly reads as following:

$$H_{CF} = \sum_{k,q} B_k^q O_k^q(J) = \sum_{k,q} A_k^q \langle r^n \rangle \theta_k O_k^q(J) \quad (1)$$

where B_k^q are the CF parameters, and O_k^q are Stevens operator equivalents which are written in the powers of the angular momentum operators, J^+ , J and J_z . A_k^q are the CF coefficients, and $\langle r^n \rangle$ is a radial distribution function of the $4f$ electrons with $k=2, 4, 6$. θ_k are operator equivalent factors for $k = 2, 4, 6$. For an orthorhombic point group as in this case, the Hamiltonian takes the following form with reduced CF parameters:

$$H_{CF} = B_2^0 O_2^0 + B_2^2 O_2^2 + B_4^0 O_4^0 + B_4^2 O_4^2 + B_4^4 O_4^4 + B_6^0 O_6^0 + B_6^2 O_6^2 + B_6^4 O_6^4 + B_6^6 O_6^6 \quad (2)$$

where the operator equivalents of O_k^q ($k, q = 2, 4, 6$) can be found in reference³⁸.

The current task is to determine the values of the B_k^q by fitting the experimental values. For a low symmetry such as orthorhombic, there are more B_k^q to be fitted. Too many independent fitting parameters in the model may cause unstable fitting and unreasonable parameter values. Starting with the initial values, which were estimated from the point-charge model,^{41,42} the CF parameters B_k^q are fitted to the experimental data using a fitting procedure developed based on the PyCrystalField package.³⁴ We use a standard, right-handed Cartesian coordinate system for the Stevens parameters with the z -axis parallel to the crystallographic c axis and the y -axis parallel to the crystallographic b axis. A set of stable parameters were achieved via this fitting procedure.

The blue curve in Fig. 3 shows the fitted excitation peaks in the experimental energy range. The fitting matches the red-dot experimental data very well (see Fig. S6 for more details). The fitted CF parameters are listed in TABLE I and the fitted CF energy levels and intensities are listed in TABLE II. Comparing these parameters to the results obtained for the orthorhombic scenario by Rudowicz et al.²⁷ we find that the fitted parameters are in a reasonable range. The fitted model gives the peaks at 0.31, 5.8, 8.74, 13.42, 18.82, 20.56 and 25.07 meV, matching the experimental data very well. The peak at 0.31 meV matches the lowest energy excitation discussed in the section above. The peak at 25.07 meV is slightly lower than the observed excitation peak. Another weak peak at 8.7 meV was not observed in the experimental data. The slight mismatches between the calculated model and the experimental data may be caused by many possible reasons, such as the imperfect model, the experimental errors, etc.

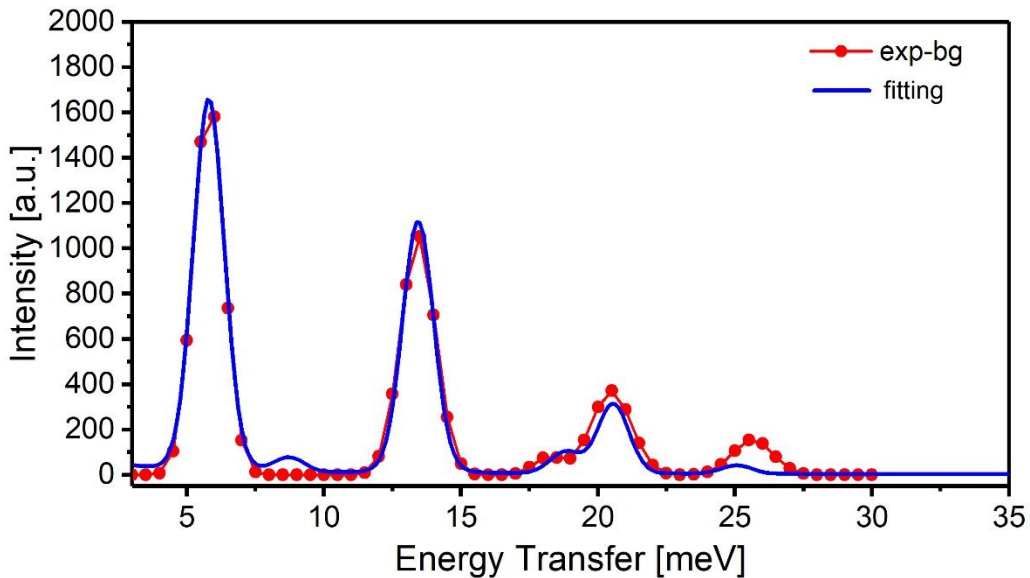


Fig. 3 The CF excitations measured in ErFeO_3 at 1.5K, which are fitted to the CF model described by the Stevens operator equivalents. The red-dot curve shows the experimental data after subtracting the background. The blue curve is the fit to the experimental data with the model described in the text for Er^{3+} in ErFeO_3 .

The energy scheme of Er^{3+} CF is plotted in Fig. 4. The obtained CF model gives seven energy levels in the energy range from 0 to 30 meV. They are at 0meV, 0.31 meV, 5.8 meV, 8.7meV, 13.4 meV, 18.8meV, 20.5 meV, and 25.1 meV. These peaks correspond to the Kramers doublets in the current compound. In our experiment, we observe a CF excitation at 7.5 meV at elevated temperature (Fig. S4), which is attributed to the excitation from 5.8 meV to 13.4 meV. Such a consistency between the model and the experiment strongly supports the validity of the CF model we proposed here.

TABLE I The fitted CF Stevens operator parameters in meV

B_2^0	B_2^2	B_4^0	B_4^2	B_4^4
-0.032(10)	-0.075(15)	-1.88(40)e-04	0.00119(18)	-0.00039(22)
B_6^0	B_6^2	B_6^4	B_6^6	
0.48(17)e-06	1.48(16)e-05	-5.94(25)e-05	0.41(54)e-05	

TABLE II The fitted CF excitation energy levels of Er^{3+} Kramers doublets in ErFeO_3

CF levels	0	1	2	3	4	5	6	7
Energy (meV)	0.0	0.31	5.8	8.74	13.44	18.82	20.56	25.07

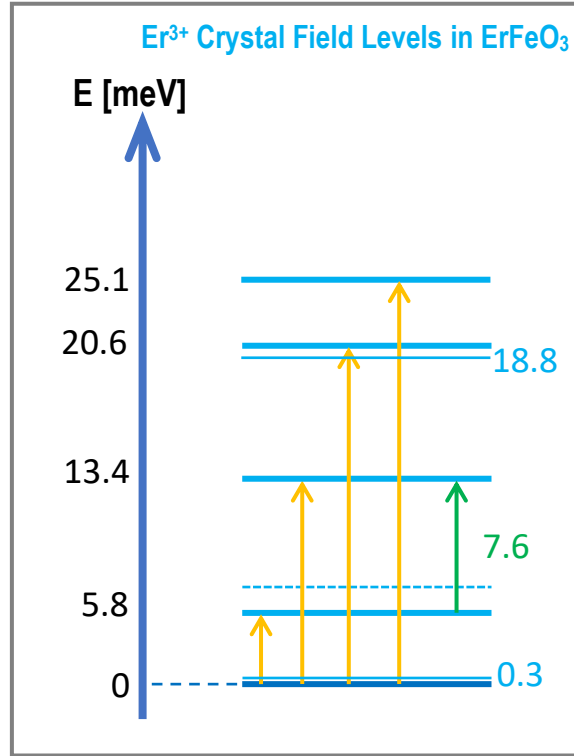


Fig. 4 Energy scheme of the CF excitations in ErFeO₃ according to the fitting to the experimental data. The solid dark-blue line at the bottom denotes the ground level of CF in ErFeO₃. The solid light-blue horizontal lines are the CF energy levels observed in experiment and refined by fitting. The dashed blue horizontal line shows the CF energy level for which we did not see evidence in the experiment but which is predicted by the crystal-field model. The orange arrows indicate the excitations from the ground state while the green arrow shows the excitation from one excited CF level to another excited CF level.

Even though the lowest CF excitation at ~ 0.3 meV which shown in Fig. 1 was not included in the data fitting procedure discussed above because the peak could be not separated from the elastic line in the Taipan experiment due to the coarse instrument resolution and the Pelican data in Fig. 1 was not able to be normalized to the Taipan data, the theoretical model still gives this excitation, as shown at ~ 0.3 meV (the first CF level in Table II). This consistency between the experimental data and theoretical model strongly support the CF model proposed above. The $^4I_{15/2}$ CF of Er³⁺ splits into a series of Kramers doublets, whose energy levels are as depicted in Fig. 4. These levels are shifted from the origin energy levels by the internal magnetic fields of Er³⁺ ordering. Especially, the splitting of the lowest Kramers doublet was significant when the Er³⁺ spins form a long-range order.

C. Effect of an external magnetic field on the crystal-field excitation of ErFeO₃

In order to investigate the origin of the energy shift of the CF excitation observed above, we conducted further inelastic neutron scattering experiments under external magnetic fields on Sika. The ErFeO₃ single crystal was mounted with the *ac* plane as the scattering plane. Vertical magnetic fields from 0 up to 10 T were applied step by step for the measurements. The magnetic field dependencies of the lowest-energy excitation

were measured at both 1.5K and 10K, below and above $T_{N(Er)}$, respectively. The results are summarized in Fig. 5. Fig. 5 (a) and (c) show the magnetic-field dependences of the CF excitation energy in the high-field region up to 10 T for the measurements taken at 1.5 K and 10 K, respectively. Fig. 5 (b) shows the low-field dependency of the CF excitation energy in the low external magnetic field range with more details.

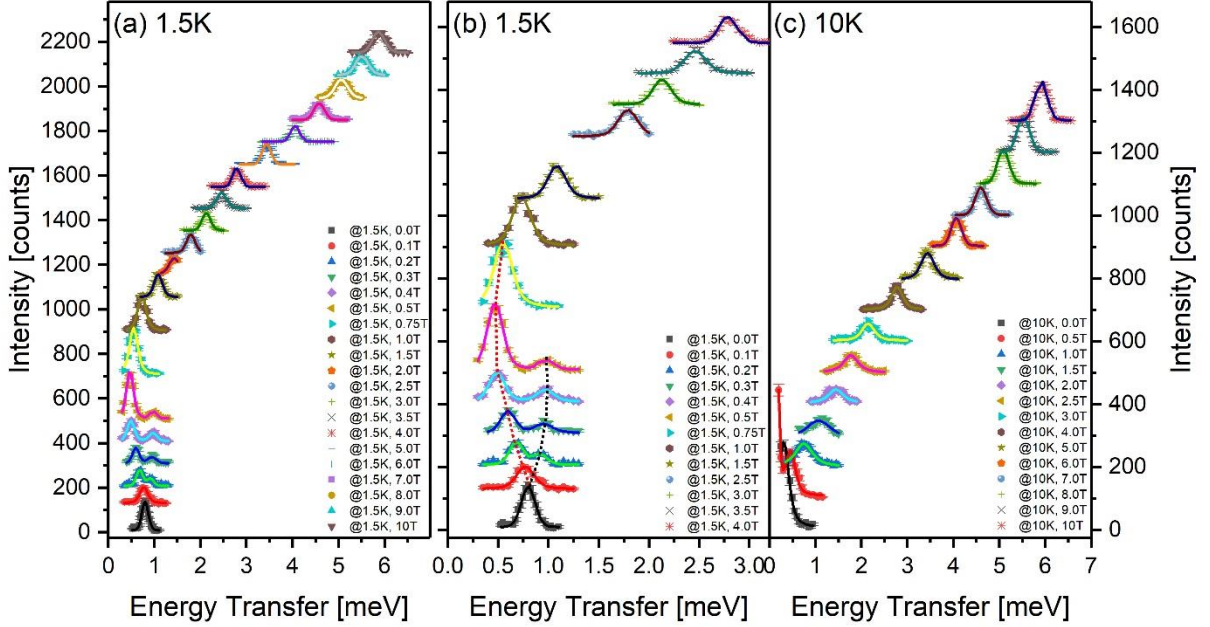


FIG 5 (colour online) Magnetic-field dependences of the low-energy CF excitation of $ErFeO_3$ were determined by conducting energy scans at $Q(1, 0, 0.5)$ on Sika at (a) (b) 1.5K and (c) 10K, i.e. below and above $T_{N(Er)}$, respectively. The magnetic fields were applied along the b axis of the $Pbnm$ crystal structure. The symbol curves in (a), (b) and (c) are the experimental data, which are fitted to the damped harmonic oscillator model by convoluting with the instrumental resolution according to the experimental configuration. The solid colour lines show the fitted curves. (b) shows the magnified low-field zone of (a) with the same intensity scale as (c). The dotted lines in (b) are guides to eyes. The scans in each of (a), (b) and (c) are offset along the vertical axis to avoid the individual scans overlapping each other.

In the C_z antiferromagnetic ordering state of Er^{3+} at 1.5K, the single peak at zero field shows a distinct splitting into two branches when applying a low magnetic field ($< 1T$). Upon increasing the external fields within this range, the energy of the upper branch gradually increases while its intensity decreases correspondingly, and the peak eventually vanishes at about 0.6 T. The energy of the lower branch first decreases from 0.75 meV to an energy level of about 0.5 meV when increasing the external magnetic fields from 0 to 0.5 T. Above 0.5T, the CF excitation energy of this branch starts to increase almost linearly with the applied external field. The data in Fig. 5(a) were fitted by convoluting with the instrumental resolution. The fitted peak positions are plotted in Fig. 6(a), in which the blue-symbol curve corresponds to the upper branch and the red one represents the lower branch. This figure clearly exhibits the linear relationship of the lower-branch energy with the applied external field in the range from 1T to 6T. The slope of this linear relationship slightly

dropped at the higher magnetic field range from 6T to 10T. At the external field up to 10T, the CF excitation peak was observed at $\sim 5.8\text{meV}$.

The results from the paramagnetic state of Er^{3+} at 10K were fitted and plotted in Fig. 5(b) by using the same convolution method and the fitted results were plotted in Fig.6(b). Major differences between the 10 K and 1.5 K data appear at magnetic fields below 1T (see Fig. 5 and 6). At 10K, no splitting of the CF excitation peak was observed under external fields, which suggests that the ordering of Er^{3+} magnetic moments caused the splitting of the lowest CF peak under external magnetic fields. Upon applying the magnetic field, the peak position shows a very similar dependency on the magnetic fields as the result observed at 1.5K in the range from 1 to 10T. Both have a linear relationship with a slope about 0.65 meV/T for from 1T to 6T, then the slope slightly drops from 6T to 10T. A similar linear relationship was previously reported for the magnetization under external magnetic fields ($\parallel b$ axis) from 0 to 6T. The slope slightly decreases in the range from 6T to higher fields, too.⁴³ According to this study, the Er^{3+} magnetic moments start to cant along the external field when the field is larger than 6T at $\sim 1.5\text{K}$. The rotation of the Er^{3+} magnetic moments could be the reason why the Zeeman splitting energy shows a nonlinear field dependency at fields higher than 6T. The linear and nonlinear field dependencies were observed at both 1.5K and 10K. The similarity between the results at 1.5K and 10K at high fields may indicate that the ordering effect of Er^{3+} on the CF excitation can be overcome by applying an external field about 1T.

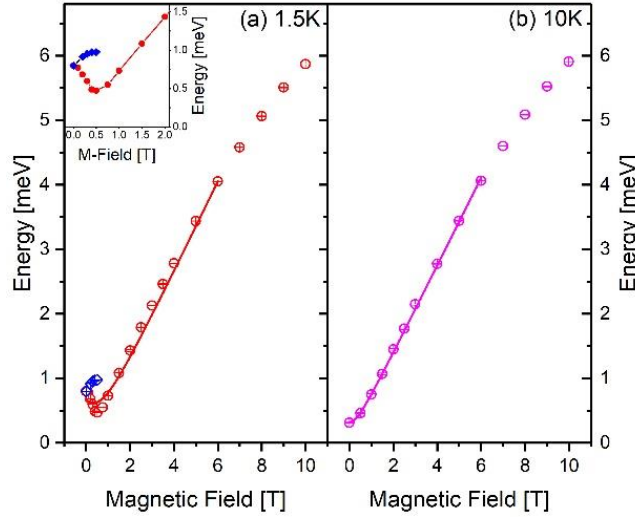


FIG. 6 (Color online) Energy of the CF excitation as function of an externally applied magnetic field along the crystallographic b direction. The symbols in (a) and (b) shows the fitted crystal-field excitation energy from the experimental data shown in Figures 5(a) and 5(b) at 1.5K and 10K, respectively. At 1.5K (a), the CF excitation splits into two peaks at low magnetic fields, which are denoted by the red and blue symbols. The red-symbol curve shows a special feature with the external magnetic field: first decreasing at the low magnetic field and then increasing at high magnetic fields. At 10K (b), the CF excitation does not split, but shifts to higher energy with the increase of the magnetic field, as shown by the magenta symbols. The red and magenta solid curves in (a) and (b) are fitted to the model described in the text. The inset in (a) shows

the zoomed-in view of the low-magnetic-field and low-energy region of (a). The upper branch of the split peak can be hardly discerned when the external magnetic field increases above 0.5T.

Differently from the three quartets and two doublets in cubic symmetry, the Er^{3+} ground state splits into eight Kramers doublets in an orthorhombic symmetry. These doublets with Kramers degeneracy can be lifted when applying an external magnetic field, or due to the internal fields induced by the long-range ordering of Er^{3+} spins. Such splitting of the degenerated doublets has been reported for many rare-earth compounds.^{44,45} For example, Iwasa *et al.* reported the splitting of the non-Kramers doublet of Pr^{3+} in $\text{PrT}_2\text{Zn}_{20}$ (T = Ir, Rh, and Ru) by using inelastic neutron scattering.⁴⁶ The splitting of the ground-state Kramers doublet of Sm^{3+} was observed at 2K by infrared spectroscopy in SmMnO_3 and was reported by Nekvasil *et al.*⁴⁷ Infrared transmission measurement was used to observe the ground-state Kramers-doublet splitting in DyMnO_3 by Jandl *et al.*¹².

The lowest CF doublet of Er^{3+} is sensitive to the internal fields in ErFeO_3 at low temperature. When the rare-earth magnetic ions form a long-range magnetic ordering, the internal field builds up and shift the energy of the CF levels. Considering both the effect of the internal and external magnetic fields, the splitting energy 2Δ of the doublet can be determined by the following formula:⁴⁴

$$\Delta^2 = \Delta_{cf}^2 + [g_{eff}\mu_B(\mathbf{H}_{ex} \pm \mathbf{H}_{in})]^2 \quad (3)$$

where Δ is the splitting energy, Δ_{cf} is the crystal field excitation energy, g_{eff} is the component of the g tensor along the field \mathbf{H} . μ_B is the Bohr magneton, \mathbf{H}_{ex} is the applied external magnetic field, and \mathbf{H}_{in} is the component of the effective internal magnetic field along \mathbf{H}_{ex} . According to Wood *et al.*,³⁷ the internal field on the Er^{3+} sites are not necessarily along the main crystallographic directions.³⁷ In addition, since the Er^{3+} magnetic moments stay in an antiferromagnetic ordering state at 1.5K, the internal field induced by the sites with moments pointing up adds to the external field while the field induced by the sites with moments pointing down subtracts from the external field, resulting in the splitting effect at the low magnetic fields < 0.5 T. When the external field is larger than the internal field, such a splitting will be overcome. Therefore, Eq. (3) has the sign \pm in front of \mathbf{H}_{in} . It is worthwhile to stress that the internal field is not necessarily along a the main crystallographic axis, and the g_{eff} factor, which is the component along the external magnetic field, is generally different for different CF levels, different magnetic fields, and different temperatures, too. Fitting the experimental data in Fig. 6 (a) and (b) to Eq. (3), we obtained the fitting parameters shown in Table III:

Table III. The fitted exchange energy, internal field and g_{eff} factor from Eq.(3) at 1.5K and 10K

T [K]	Δ_{cf} (meV)	H_{in} (meV)	g_{eff}
10	0.32 (3)	0	11.79(5)
1.5	0.62 (5)	0.33 (13)	12.20 (28)

The second row of Table III shows the fitted parameters from the data at 10K. At this temperature, we set the parameter H_{in} to zero and the fit gives $\Delta_{cf} = 0.32 \pm 0.025\text{meV}$ and the g_{eff} component = 11.79. The Δ_{cf} value is consistent with the observed energy gap at 10K, which is about 0.35 meV. The g_{eff} factor is substantially larger than the theoretical values of 5.6 (Γ_6) or 6.8 (Γ_7) proposed in reference³⁹, which indicates the strong spin-orbital coupling of Er^{3+} ions in this magnet.

At 1.5K, the Er^{3+} spins form a long-range antiferromagnetic ordering state. The internal field from the Er^{3+} ordering is applied to the CF doublets. Fitting Eq. (3) to the experimental data at 1.5K generates the parameters listed in the third row of Table III. The excitation energy Δ_{cf} is ~ 0.62 meV, the internal field $H_{in} \sim 0.33\text{meV}$ and $g_{eff} \sim 12.2$. Δ_{cf} is much larger at 1.5K than at 10K. The internal field H_{in} induced by the ordered Er^{3+} moments is comparable to the difference between the two values of Δ_{cf} at 1.5K and 10K. The g_{eff} values at both 1.5K and 10K are almost the same and much larger than the reported g_{eff} values at 77K and the theoretical values.³⁷ Similar large g_{eff} values have been reported previously,³⁹ which is mainly due to the large anisotropy of the g_{eff} factor induced by the spin-orbital coupling.

As known from above, the CF of ErFeO_3 splits into eight doublets due to the local symmetry of ErFeO_3 . The lowest-energy excitation below 1meV at zero magnetic field is shifted to the higher energy by the internal field induced by the ordering of the Er^{3+} magnetic moments when the sample is cooled below $T_{N(Er)}$. Applying low external fields at 1.5K can split this excitation further in two peaks due its Kramers-doublet nature. The Zeeman splitting below $T_{N(Er)}$ was investigated by using Mössbauer spectroscopy, resulting in ~ 0.66 meV at 1.5K and ~ 0.28 meV at 4.2K, these values are very close to the values we observed: 0.75 meV at 1.5K and 0.35 meV at 4.5K.⁴⁸ This agreement strongly supports our interpretation of the origin of the low-energy excitation.

Similar energy shifts were observed for the other CF excitation levels in ErFeO_3 . For example, we observed energy shifts with temperature for the CF peak at 5.5meV, as shown in Fig. S5(a). The big shift step ($\sim 0.33\text{meV}$) from 1.5K to 10K should be ascribed to the internal field variation caused by the Er^{3+} ordering while the second step ($\sim 0.1\text{meV}$) from 80K to 100K is due to the internal-field change of the Fe^{3+} sublattice (see Fig. S5). This indicates that the ordering of Er^{3+} moments and spin reorientation of Fe^{3+} moments strongly affect the CF excitations. To some extent, the effect of the ordered Fe^{3+} moments on the crystal-field excitation of Er^{3+} cannot be excluded in the whole temperature range. Apparently, this effect is smaller than the one from Er^{3+} .

IV. CONCLUSION

The crystal field excitations were systematically measured in ErFeO_3 at different temperatures and in external fields using the inelastic neutron scattering technique. A large energy shift of the lowest-energy CF excitation in ErFeO_3 was observed when the sample cools down through the antiferromagnetic phase transition of Er^{3+} spins. A CF model was proposed for Er^{3+} in ErFeO_3 by fitting to the CF peaks collected. According to the model, we found that the large energy shift of the CF excitation is induced by the internal field of the or-

dered phase of Er^{3+} spins. With the experimental data in the magnetic fields, the internal field of Er^{3+} ordering state is extracted by fitting the data to the Zeeman splitting model. The large field dependency of the crystal-field excitation is attributed to the large anisotropy of the g_{eff} factor and large g_{eff} component along the b axis. Our results provide valuable information for the understanding of competing interactions between the rare-earth ions and transition-metal ions in TMO materials.

ACKNOWLEDGMENTS

We would like to thank Drs. Richard, Mole (ANSTO), Rob Robinson and G. Khaliullin (Max Planck Institute for Solid State Research, Stuttgart,) for fruitful discussions. We thank ANSTO for the allocation of neutron beam time on Taipan, Sika and Pelican (P3169, P3847, P5242, P5295). This work was financially supported by the National Natural Science Foundation of China (NSFC, Nos. 11774217, 12074242, 12074241), the Australian Institute of Nuclear Science and Engineering Ltd (AINSE) and the Australian Research Council (ARC) through the funding of the Discovery Grants DP110105346 and DP160100545.

REFERENCES

- ¹ B. Lorenz, *ISRN Condensed Matter Physics* **2013**, 497073 (2013).
- ² L. Balents, *Nature* **464**, 199 (2010).
- ³ G. Deng, P. Guo, W. Ren, S. Cao, H. E. Maynard-Casely, M. Avdeev, and G. J. McIntyre, *Journal of Applied Physics* **117**, 164105 (2015).
- ⁴ R. L. White, *Journal of Applied Physics* **40**, 1061 (1969).
- ⁵ C. Rudowicz and M. Lewandowska, *Spectrochimica Acta Part A: Molecular and Biomolecular Spectroscopy* **103**, 282 (2013).
- ⁶ M. Loewenhaupt and F. Steglich, edited by A. Furrer (Plenum Press, New York, 1977).
- ⁷ R. Feile, M. Loewenhaupt, J. K. Kjems, and H. E. Hoenig, *Physical Review Letters* **47**, 610 (1981).
- ⁸ B. Frick and M. Loewenhaupt, *Zeitschrift für Physik B Condensed Matter* **63**, 213 (1986).
- ⁹ C. Rettori, E. Weber, J. P. Donoso, F. C. G. Gandra, and G. E. Barberis, *Solid State Communications* **39**, 1025 (1981).
- ¹⁰ S. Jandl, P. Richard, V. Nekvasil, D. I. Zhigunov, S. N. Barilo, and S. V. Shiryayev, *Physica C: Superconductivity* **314**, 189 (1999).
- ¹¹ S. Jandl, V. Nekvasil, M. Diviš, A. A. Mukhin, J. Hölsä, and M. L. Sadowski, *Physical Review B* **71**, 024417 (2005).
- ¹² S. Jandl, S. Mansouri, J. Vermette, A. A. Mukhin, V. Y. Ivanov, A. Balbashov, and M. Orlita, *Journal of Physics: Condensed Matter* **25**, 475403 (2013).
- ¹³ A. T. Boothroyd, S. M. Doyle, D. M. Paul, and R. Osborn, *Physical Review B* **45**, 10075 (1992).
- ¹⁴ K. W. Becker, P. Fulde, and J. Keller, *Zeitschrift für Physik B Condensed Matter* **28**, 9 (1977).
- ¹⁵ E. A. Goremychkin, R. Osborn, B. D. Rainford, E. D. Bauer, M. B. Maple, and M. Koza, *Physica B: Condensed Matter* **378-380**, 58 (2006).

- ¹⁶ R. K. Oogarah, C. P. J. Stockdale, C. Stock, J. S. O. Evans, A. S. Wills, J. W. Taylor, and E. E. McCabe, *Physical Review B* **95**, 174441 (2017).
- ¹⁷ E. A. Goremychkin, R. Osborn, C. H. Wang, M. D. Lumsden, M. A. McGuire, A. S. Sefat, B. C. Sales, D. Mandrus, H. M. Rønnow, Y. Su, and A. D. Christianson, *Physical Review B* **83**, 212505 (2011).
- ¹⁸ M. Diviš, J. Hölsä, M. Lastusaari, A. P. Litvinchuk, and V. Nekvasil, *Journal of Alloys and Compounds* **451**, 662 (2008).
- ¹⁹ A. A. Sirenko, S. M. O'Malley, K. H. Ahn, S. Park, G. L. Carr, and S. W. Cheong, *Physical Review B* **78**, 174405 (2008).
- ²⁰ K. P. Belov, A. K. Zvezdin, A. M. Kadomtseva, and R. Z. Levitin, *Sov. Phys. Usp.* **19**, 574 (1976).
- ²¹ S. Cao, L. Chen, W. Zhao, K. Xu, G. Wang, Y. Yang, B. Kang, H. Zhao, P. Chen, A. Stroppa, R.-K. Zheng, J. Zhang, W. Ren, J. Íñiguez, and L. Bellaiche, *Sci. Rep.* **6**, 37529 (2016).
- ²² Y. Cao, M. Xiang, W. Zhao, G. Wang, Z. Feng, B. Kang, A. Stroppa, J. Zhang, W. Ren, and S. Cao, *J. Appl. Phys.* **119**, 063904 (2016).
- ²³ H. Wu, S. Cao, M. Liu, Y. Cao, B. Kang, J. Zhang, and W. Ren, *Phys Rev B* **90**, 144415 (2014).
- ²⁴ Y. Tokunaga, S. Iguchi, T. Arima, and Y. Tokura, *Phys Rev Lett* **101**, 097205 (2008).
- ²⁵ A. V. Kimel, A. Kirilyuk, A. Tsvetkov, R. V. Pisarev, and T. Rasing, *Nat.* **429**, 850 (2004).
- ²⁶ S. M. Shapiro, J. D. Axe, and J. P. Remeika, *Phys Rev B* **10**, 2044 (1971).
- ²⁷ C. Rudowicz and P. Gnutek, *Spectrochimica Acta Part A* **79**, 60 (2011).
- ²⁸ M. P. Zic, W. T. Fuhrman, K. Wang, S. Ran, J. Paglione, and N. P. Butch, *J. Appl. Phys.* **130** 014102 (2021).
- ²⁹ C.-M. Wu, G. Deng, J. S. Gardner, P. Vorderwisch, W.-H. Li, S. Yano, J.-C. Peng, and E. Imamovic, *Journal of Instrumentation* **11**, 10009 (2016).
- ³⁰ S. A. Danilkin and M. Yethiraj, *Neutron News* **20**, 37 (2009).
- ³¹ D. Yu, R. A. Mole, and G. J. Kearley, *EPJ Web of Conferences* **83**, 03019 (2015).
- ³² J. W. Eaton, D. Bateman, S. Hauberg, and R. Wehbring, (CreateSpace Independent Publishing Platform, 2014).
- ³³ Reslib, <https://neutron.ethz.ch/research/resources/reslib.html>.
- ³⁴ A. Scheie, *Journal of Applied Crystallography* **54**, 356 (2021).
- ³⁵ P. Čermák, A. Schneidewind, B. Liu, M. M. Koza, C. Franz, R. Schönmann, O. Sobolev, and C. Pfleiderer, *Proceedings of the National Academy of Sciences* **116**, 6695 (2019).
- ³⁶ S. L. Gnatchenko, I. S. Kachur, V. S. Kurnosov, V. G. Piryatinskaya, A. V. Malakhovskii, and I. A. Gudim, *Phys. Rev. B* **45**, 928 (2019).
- ³⁷ D. L. Wood, L. M. Holmes, and J. P. Remeika, *Physical Review* **185**, 689 (1969).
- ³⁸ S. Laachir, M. Moussetad, R. Adhiri, and A. Fahli, *Z. Naturforsch* **66a**, 457 (2011).
- ³⁹ C. A. J. Ammerlaan and I. d. Maat-Gersdorf, *Appl. Magn. Reson.* **21**, 13 (2001).
- ⁴⁰ J. e. J. Baldov, S. Cardona-Serra, J. M. Clemente-Juan, E. Coronado, A. GaitaArino, and A. Pali, *Journal of Computational Chemistry* **34**, 1961 (2013).
- ⁴¹ S. Edvardsson and M. Klintonberg, *Journal of Alloys Compounds* **275**, 230 (1998).
- ⁴² J. Mesot and A. Furrer, *Journal of Superconductivity* **10**, 623 (1997).
- ⁴³ X. X. Zhang, Z. C. Xia, Y. J. Ke, X. Q. Zhang, Z. H. Cheng, Z. W. Ouyang, J. F. Wang, S. Huang, F. Yang, Y. J. Song, G. L. Xiao, H. Deng, and D. Q. Jiang, *Physical Review B* **100**, 054418 (2019).
- ⁴⁴ J. Hemberger, M. Brando, R. Wehn, V. Y. Ivanov, A. A. Mukhin, A. M. Balbashov, and A. Loidl, *Physical Review B* **69**, 064418 (2004).
- ⁴⁵ E. C. Standard, T. Stanislavchuk, A. A. Sirenko, N. Lee, and S. W. Cheong, *Physical Review B* **85**, 144422 (2012).
- ⁴⁶ K. Iwasa, H. Kobayashi, T. Onimaru, K. T. Matsumoto, N. Nagasawa, T. Takabatake, S. Ohira-Kawamura, T. Kikuchi, Y. Inamura, and K. Nakajima, *Journal of the Physical Society of Japan* **82**, 043707 (2013).
- ⁴⁷ V. Nekvasil, S. Jandl, A. A. Mukhin, V. Y. Ivanov, and A. M. Balbashov, *Phys. Rev. B* **105**, 07E113 (2009).

⁴⁸ L. A. Prelorendjo, C. E. Johnson, M. F. Thomas, and B. M. Wanklyn, *J. Phys. C: Solid State Phys.* **15**, 3199 (1982).

Supplemental Material: Giant shifts of crystal-field excitations in ErFeO₃ driven by internal magnetic fields

Joel O'Brien,¹ Guochu Deng,^{2*} Xiaoxuan Ma,³ Zhenjie Feng,³ Wei Ren,³ Shixun Cao,^{3†} Dehong Yu,² Garry J McIntyre,² Clemens Ulrich¹

¹ School of Physics, The University of New South Wales, Kensington, NSW 2052, Australia

² Australian Centre for Neutron Scattering, Australian Nuclear Science and Technology Organisation, New Illawarra Road, Lucas Heights, NSW 2234, Australia

³ Department of Physics, International Centre of Quantum and Molecular Structures and Materials Genome Institute, Shanghai University, Shangda Road 99, Shanghai 200444, People's Republic of China

Inelastic neutron experiments were conducted on the cold-neutron triple-axis spectrometer Sika to study the excitations from ErFeO₃. With the *ac* plane as the scattering plane, an excitation peak was observed below the ordering temperature $T_{M(\text{Er})}$ of Er³⁺ spins. Following this discovery, a series of energy scans at temperatures from 1.7K to 10K were performed at $Q = (1\ 0\ 0.5)$ of ErFeO₃. The results are plotted in Fig. S1. It is clearly seen that a low-energy excitation at ~ 0.35 meV at 10 K gradually evolves to higher energy, reaching 0.7 meV around 1.7K. A further experiment with higher energy resolution was carried out on the time-of-flight spectrometer Pelican, showing almost the same trend of the energy change of this excitation with the slightly higher energy resolution in Fig. 1 in the main article.

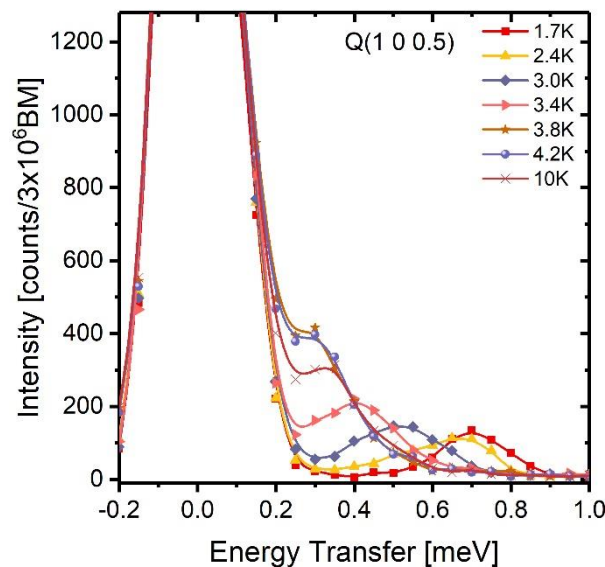


FIG. S1 Low-energy scans at $Q (1\ 0\ 0.5)$ of ErFeO₃ at different temperatures on Sika. The symbol lines are the experimental data collected on Sika. The line curves are the fitting to the experimental data by convoluting with the instrument resolution of Sika in the configuration used for the experiment.

* Corresponding Author: guochu.deng@ansto.gov.au

† Corresponding Author: sxcao@shu.edu.cn

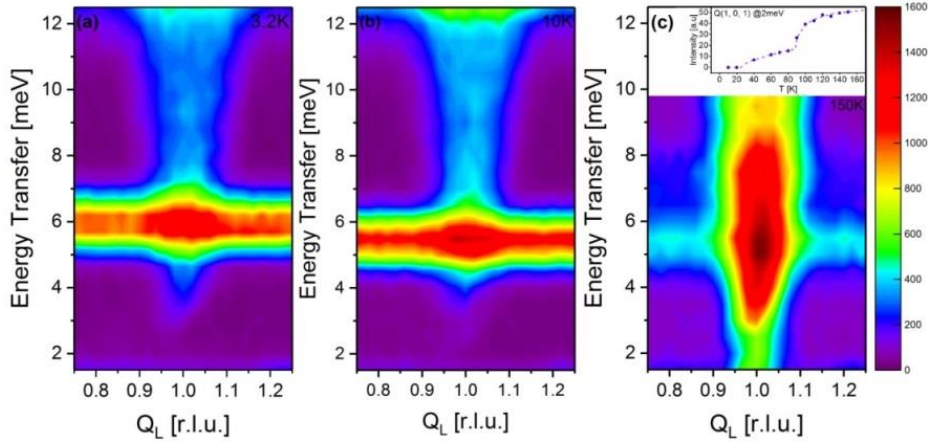


FIG. S2 False-colour contour maps of the spin gap and CF excitations of ErFeO_3 near the antiferromagnetic zone centre $Q = (1\ 0\ 1)$ measured at (a) 1.5K, (b) 10K and (c) 150K. The inset in (c) shows the temperature dependency of the inelastic intensity at the energy transfer of 2meV at the zone centre, indicating the three different zones of the excitation.

Further measurements with wide energy transfers were conducted on Sika to study the crystal-field excitations in ErFeO_3 at low temperatures. The measurements mainly focused on the Q range in the vicinity of the antiferromagnetic (AFM) zone centre $(1\ 0\ 1)$ of ErFeO_3 in the energy regime below 10 meV. Fig. S2(a), (b) and (c) present the low-energy spectrum maps from the ErFeO_3 single crystal near the AFM zone centre $(1\ 0\ 1)$ at 1.5K, 10K and 150K, respectively. There are two main discernible excitation features in these figures. The first feature is the spin-wave excitation at the zone centre, which is vertically distributed in a relatively narrow Q space at low energy and slightly broadens at higher energy, indicating a very-sharp spin-wave dispersion, consistent with the previous reports in other orthoferrites. An energy gap of about 3 meV is observed at 1.5K and 10K. The spin-wave excitation does not show significant changes when heating from 1.5K to 10K while its intensity is obviously enhanced at 150K and the energy gap narrows (less than 2meV) at the same time due to the suppressed magnetic single-ion anisotropy on heating. Such changes can be clearly identified in Fig. S3 (a), (b) and (c), too, which show two energy scans at the zone centre and off-centre Q positions at 1.5K, 90K and 150K, respectively. The intensity of the zone-centre scan between 1 meV and 3 meV significantly increases when the temperature rises to 90 K and 150 K.

The inset of Fig. S2(c) shows the temperature dependency of the constant energy scan at 2meV near the zone centre. Three different regions are clearly discerned in temperature: below 20K, there is no signal at all; in the region $20\text{K} < T < T_i$, the intensity gradually increases and saturates when approaching T_i ; above T_u , the intensity quickly increases and become nearly saturated around 150K. This curve shows a clear kink at the spin-reorientation phase transition of the Fe^{3+} magnetic phase,

indicating that the spin-reorientation phase transition is strongly correlated to the single-ion anisotropy of the system.

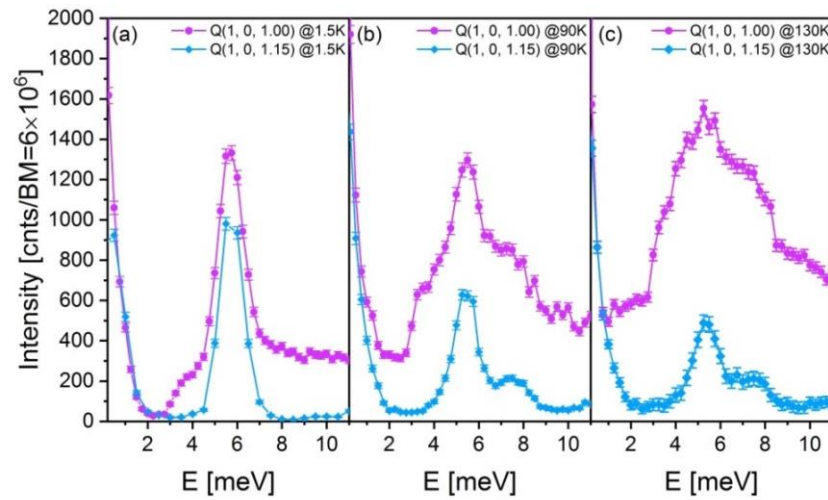


FIG. S3 Energy scans at the zone centre Q (1 0 1) and Q (1 0 1.15) at (a) 1.5K, (b) 90K and (c) 150K.

The second feature in the data of Fig. S2 is the strong excitation around 5.5 meV, which shows no dispersion along Q and is safely ascribed to the CF excitation. From the data at 1.5K, 90K and 130K in Fig. S3, we found that this CF excitation slightly shifted in energy with the change of temperature. The excitation energy decreases from ~ 5.8 meV at 1.5 K to ~ 5.4 meV at 90K, indicating the strong effect from the long-range ordering of Er^{3+} magnetic moments. Rising from 1.5K to 90K, and then to 150K, the peak intensity drops, and a shoulder shows up at ~ 7.5 meV on the high-energy side of this CF peak, which was not observed at 1.5 K.

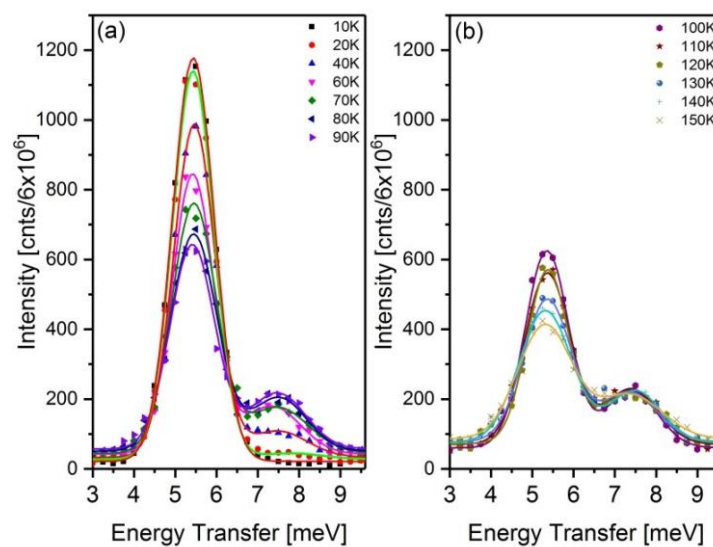


FIG. S4 Energy scans at the off-centre Q (1 0 1.15) position at different temperatures. The peaks in the data are fitted by convoluting with the instrument resolution of Sika.

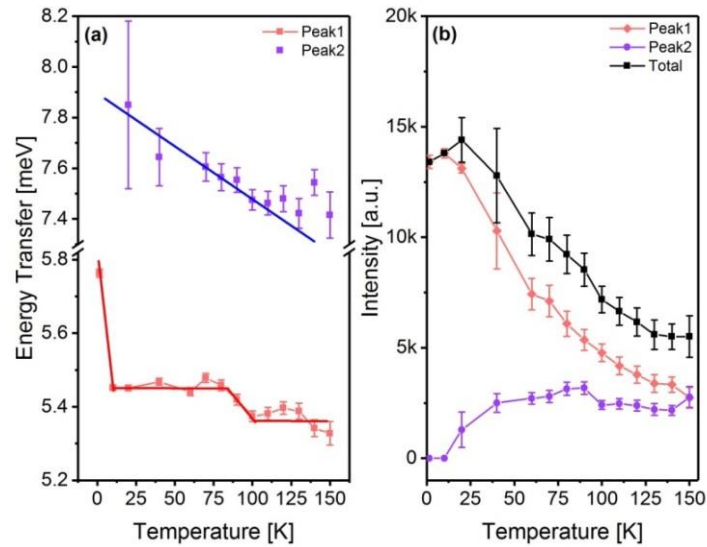


FIG. S5 The temperature dependency of the fitted peak positions (a) and intensities (b) from the energy scans in Fig. S4. The thick lines in (a) are guides to the eyes; the thick lines in (b) simply connect the data points.

A more detailed temperature dependency of the CF peak was measured in order to clarify the reason for the energy shift observed above. Fig. S4 (a) and (b) show the measured results of these two peaks at a series of temperatures from 10K to 150K. The data were well fitted by two Lorentzians convoluted with the instrument resolution. The fitted peak positions and intensities are plotted in Fig. S4. The red and purple curves in Fig. S5(a) show the two excitation energies at different temperatures. At 1.5K, below $T_{N(E_r)}$, the excitation energy is around 5.75meV, a value much higher than those at higher temperatures. This excitation energy shows three steps in the full temperature range: ~ 5.75 meV below $T_{N(E_r)}$, ~ 5.5 meV from $T_{N(E_r)}$ to T_l , and ~ 5.35 meV above T_u . The shoulder peak at 7.5meV (purple curve) shows a slightly different temperature dependency. The intensity gradually increases with the rise of the temperature from 1.5K to 90K, and almost saturates above 90K. The peak energy gradually decreases on heating (see Fig. S5(b)). These two features indicate that this peak corresponds to an excitation from one excited state to another higher-energy excited state.

Fig. S5(b) shows the intensity of the two excitation peaks. We can see that the main peak intensity (red curve) at 5.5 meV continuously decreases with increasing temperature while the secondary peak intensity (purple curve) increases in a stepwise fashion. The intensity is nearly zero at low temperature and gradually increases with the increase of temperature until T_l . The intensity of this peak suddenly drops above T_u . The sum of the two peak intensities (black curve) still follows a gradual decrease upon heating to higher temperature.

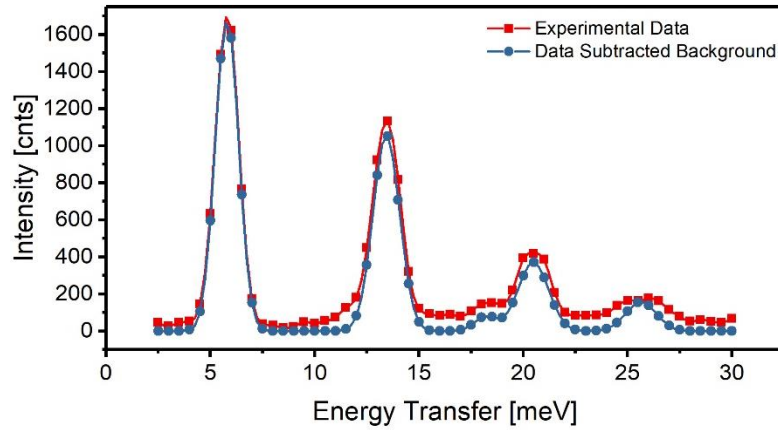


FIG. S6 The wide energy scan (red) from ErFeO_3 single crystal at 1.5K on the thermal neutron triple-axis spectrometer Taipan. The peaks in the red curve are fitted to Voigt profile functions. The difference between the fitted peaks and the experimental data are subtracted from the original data as the background. The blue curve is the data which is generated by subtracting the background from the experimental data.

Fig. S6 shows the energy scan used for the crystal field model fitting described in the main article. Since the Fe^{3+} magnetic ordered phase has a sharp spin-wave spectrum with the band top up to 60meV, it gets slightly broader with the increase of the energy transfer. Thus, it gives gradually increased background in the high energy range of the energy scan in Fig. S6. This background is removed by the method described in the legend of the figure to make a good fit to the crystal field excitations.